CRYSTAL GROWTH & DESIGN

Article

pubs.acs.org/crystal

Understanding the Competition between Epitaxial Strain and Thermodynamics in TiO_2: Structural, Morphological, and Property Evolution

Brent A. Apgar and Lane W. Martin*

Department of Materials Science and Engineering and Materials Research Laboratory, University of Illinois, Urbana-Champaign, Urbana, Illinois 61801, United States

International Institute for Carbon Neutral Energy Research, 744 Motooka, Nishi-ku, Fukuoka 819-0395, Japan

Supporting Information

ABSTRACT: We explore the evolution of epitaxial TiO_2 films on a wide range of (001)-oriented perovskite substrates. We observe epitaxial stabilization of anatase to >150 °C above the bulk anatase-to-rutile transition temperature for films grown on substrates with −2.0% to 6.0% lattice mismatch. Continuum elastic models are used to calculate the strain energy density and to construct a model for the preferred epitaxial orientation of anatase. This model is consistent with experimental observations that the strain energy density dominates and leads to the stabilization of 00*l*- and *h*00-oriented anatase below and above lattice mismatch values of 5%, respectively. Additionally, TiO_2 nanocrystallite size is found to decrease with lattice mismatch and is discussed in terms of energy competition and possible changes in the nucleation and growth process. To further probe the competition between bulk free, surface, interface, and strain energies in metastable (kinetically limited) as-grown TiO_2 films, ex post facto annealing was completed to assess the equilibrium state of the films. These studies confirm the continuum elastic model and highlight the relative importance of the different energies. We then implement our understanding of energy competition to deterministically increase surface area and enhance light absorption via in situ growth processes and ex post facto annealing.

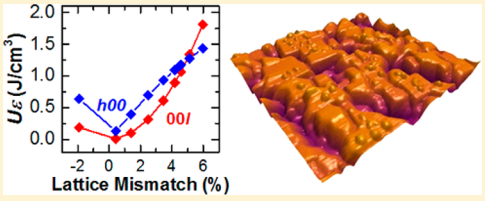

1. INTRODUCTION

TiO_2 is one of the most widely studied binary oxides and is known to exhibit three structural polymorphs: anatase, rutile, and brookite. Of these, only rutile is the thermodynamically stable phase, anatase converts irreversible to rutile at ∼750 °C, and brookite is observed only in mineral form when stabilized by dopants or as an intermediate phase during anatase crystallization.[1] Anatase, because of its chemical stability, photoinduced hydrophilicity, and earth abundance, has been studied extensively as a photocatalyst and antifog coating.[2,3] While a significant body of work exists on epitaxial anatase, the authors are aware of no systematic study of such a large range of lattice mismatch on the orientation, morphology, and optical properties of this widely studied material nor of a detailed analysis of the thermodynamic competition in energies of epitaxial TiO_2.

Anatase TiO_2 (a = 3.7852 Å, c = 9.5139 Å)[4] grows epitaxial cube-on-cube, 00*l*-oriented on cubic substrates when the film−substrate lattice mismatch is small (e.g., on $LaAlO_3$, a = 3.79 Å) and epitaxial cube-on-cube *h*00-oriented anatase when the lattice mismatch is large (e.g., on MgO, a = 4.21 Å).[5,6] These observations have been explained as the result of epitaxial stabilization of anatase by the substrate, a concept easily illustrated by comparing the lattice mismatch between the substrate and anatase to that between the substrate and rutile.[7] For growth on $LaAlO_3$ (001), 00*l*-oriented anatase has only a +0.1% mismatch, while for rutile (with a = 4.59 Å, c = 2.96 Å)[4] the most commensurately matched epitaxial orientation (00*l*-oriented) has a +16.7% mismatch with $LaAlO_3$ (001) and for growth on MgO (001), *h*00-oriented anatase has a −11.5% mismatch, while 00*l*-oriented rutile has a 29.6% mismatch. Similar findings have been reported for TiO_2 grown on the perovskite substrate $SrTiO_3$.[8,9]

In this work, we provide a systematic investigation of the epitaxial growth of TiO_2 on perovskite substrates. Such epitaxial growth can extend the stability of anatase formation by at least 150 °C beyond the bulk anatase-to-rutile transition temperature regardless of the lattice mismatch within the range of −2.0% to 6.0% studied herein. Application of a continuum elastic model enables the calculation of strain energy density and a prediction of the preferred epitaxial orientation of anatase on perovskite substrates. Subsequent experimental studies reveal that this model is consistent with experimental observations that the strain energy density is the dominate energy and leads to the stabilization of 00*l*- and *h*00-oriented anatase below and above lattice mismatch values of 5%, respectively. As the lattice mismatch is increased, the TiO_2 nanocrystallite size is found to decrease, and this observation is discussed in terms of partial

Received: January 18, 2014
Revised: February 26, 2014
Published: March 5, 2014

   dx.doi.org/10.1021/cg5000974 | *Cryst. Growth Des.* 2014, 14, 1981−1988

compensation of the strain energy with surface energy and with consideration of possible changes in the nucleation and growth process. We further probe the competition between bulk free, surface, interface, and strain energies in such metastable (kinetically limited) as-grown TiO_2 films using ex post facto annealing to assess the equilibrium state of the films. These studies confirm the continuum elastic model and highlight the relative importance of the different energies in the evolution of the film structure and morphology. Finally, we implement our understanding of energy competition to deterministically increase surface area and enhance light absorption of anatase TiO_2 via in situ growth processes (completed both above and below the anatase-to-rutile transition temperature) and via ex post facto annealing (at temperatures above the transition temperature). Using these approaches, we increase the surface area of epitaxial anatase films by 20% and increase the light absorption above the band gap by 80%.

2. EXPERIMENTAL SECTION

Epitaxial thin films of 50-nm-thick TiO_2 were grown by pulsed-laser deposition from a ceramic rutile TiO_2 target using a KrF excimer laser (λ = 248 nm). The deposition was carried out in an on-axis geometry with a target-to-substrate distance of 6.3 cm; the target was sanded and cleaned prior to each deposition and sufficiently preablated to ensure uniform deposition. The resulting growth rate at a laser frequency of 16 Hz and a laser fluence of 1.35 J/cm^2 was 1.9 Å/s, which is consistent with previous studies of pulsed-laser deposition growth of TiO_2.[6,10,11] The films were grown at substrate temperatures of 600−900 °C in a dynamic oxygen ambient with a pressure of 100 mTorr, and following growth the films were cooled to room temperature in 760 Torr of oxygen at 5 °C/min. For this study, the TiO_2 films were grown on a range of perovskite single-crystal substrates including $YaAlO_3$ (110) (a_{pc} = 3.71 Å), $LaAlO_3$ (001) (a = 3.79 Å), $NdGaO_3$ (110) (a_{pc} = 3.86 Å), $(LaAlO_3)_{0.3}$-$(Sr_2AlTaO_6)_{0.7}$ (001) (LSAT, a = 3.87 Å), $DyScO_3$ (110) (a_{pc} = 3.94 Å), $TbScO_3$ (110) (a_{pc} = 3.96 Å), $GdScO_3$ (110) (a_{pc} = 3.97 Å), and $NdScO_3$ (110) (a_{pc} = 4.01 Å) substrates (CrysTec, GmbH) to probe the effect of lattice mismatch on the TiO_2 growth. The lattice mismatch of each substrate with anatase TiO_2 is shown graphically (Figure 1a). Additionally, we investigated the phase stability and morphology evolution of the epitaxial TiO_2 by ex post facto annealing studies completed at 900 °C in 760 Torr O_2 for 1−20 h. Following deposition and each annealing step, the films were characterized by X-ray diffraction (XRD) (PANalytical, X'pert MRD Pro) and atomic force microscopy (AFM) (Asylum Research, MFP-3D and Cypher). We measured the optical properties of the films grown on $LaAlO_3$ substrates before and after annealing by normal-incidence UV−visible transmission/reflection (Cary 5G).

3. RESULTS AND DISCUSSION

3.1. Preferred Epitaxial Orientation and Energetic Competition. The concept of a coincident-site lattice (CSL), while formally defined only for materials of the same crystal structure, may be extended to predict the preferred epitaxial orientation (PEO) of a thin film even when the film and substrate do not inhabit the same crystal structure, as in the case of Fe_2O_3 on $SrTiO_3$.[12] In this way, the PEO of TiO_2 on each substrate may be predicted, and for the substrates chosen here, the anatase polymorph possesses the most CSL. Additionally, previous studies have demonstrated anatase to be the preferred phase when TiO_2 is grown on cubic (or pseudocubic) (001)-oriented, single-crystal substrates, the explanation for which has uniformly been that the substrate epitaxially stabilizes this phase.[7]

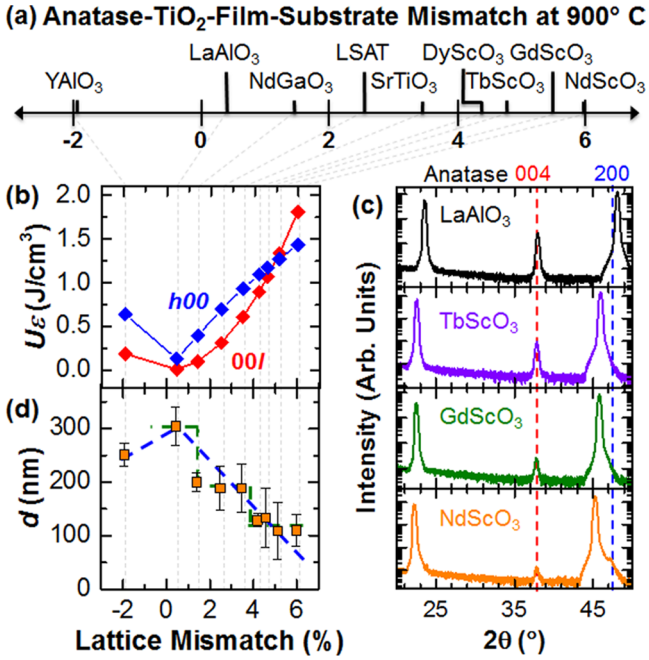

Figure 1. (a) Number line showing the lattice mismatch between anatase TiO_2 and the various (001)-oriented perovskite substrates studied in this work at the growth temperature of 900 °C. (b) Calculated strain energy density (U_ε) of the films as a function of lattice mismatch assuming a continuum elastic model. (c) θ−2θ X-ray diffraction scans of representative TiO_2 films. (d) Diameter (d) of the nanocrystallites composing the TiO_2 films as a function of lattice mismatch. Lines are drawn to guide the eye for a linear (blue) and step (green) dependence of the nanocrystallite size with lattice mismatch.

To further explore the nature of epitaxy in TiO_2-perovskite couples, we have constructed a simple continuum elastic model with which we calculate the strain energy density (U_ε) for both 00l- and h00-oriented anatase TiO_2 thin films grown on single-crystal substrates. The constitutive equation is

$$U_\varepsilon = \frac{E}{(1-\nu)\varepsilon^2} \quad (1)$$

where E is the Young's modulus (204 and 103 GPa for 00l- and h00-orientations, respectively[13]), ν is the Poisson's ratio (0.60 and 0.30 for 00l- and h00-orientations, respectively, as calculated from the published compliance tensor for anatase[13] using the relationships $\nu_{13} = S_{31}/S_{11}$ and $\nu_{31} = S_{13}/S_{33}$), and ε is the lattice mismatch at the growth temperature of 900 °C (calculated as $(a_s - a_f)/a_f$ where a_s and a_f are the lattice parameters for the substrate and film at 900 °C, respectively).[14−19] The fits for both 00l- and h00-orientations of anatase TiO_2 on the various perovskite substrates of interest are provided (Figure 1b). As can be seen from this analysis, films with 00l-orientation are preferred in the lattice mismatch regime from −2.0% to 5.0%, and beyond this value (corresponding to growth on $GdScO_3$ and $NdScO_3$ substrates in this work) films with h00-orientation are preferred due to the lower strain energy density.

From here we proceed to test this simple model of epitaxial growth by synthesizing the films of interest (unless otherwise noted, we will focus on films grown at 900 °C). Subsequent θ−2θ XRD scans of the TiO_2 films on the various substrates have been completed and (for brevity) we show the data for those grown on the substrate with the least lattice mismatch (i.e.,

dx.doi.org/10.1021/cg5000974 | Cryst. Growth Des. 2014, 14, 1981−1988

$LaAlO_3$, black data Figure 1c) and those grown on substrates in the vicinity of the strain energy crossover point (i.e., $TbScO_3$ (4.6%, purple data), $GdScO_3$ (5.1%, green data), and $NdScO_3$ (6.0%, orange data), Figure 1c). In all cases, only diffraction peaks corresponding to anatase TiO_2 are observed despite the fact that the growth took place at 150 °C above the bulk anatase-to-rutile phase transition temperature. As can be seen, the continuum elastic model yields a remarkably accurate prediction of the experimental observations in that only 00*l*-oriented anatase is observed on all substrates with the exception of $NdScO_3$ where a mixture of both 00*l*- and *h*00-oriented anatase are present. Later we will address additional energy terms (namely, surface energy) that are responsible for the mixed-phase structure of the films on $NdScO_3$. It is known that the competition between bulk volumetric and surface energies has a strong influence on the anatase-to-rutile phase transition temperature and likely becomes more important near the strain energy density crossover point.[21,22]

XRD pole figure studies (Supporting Information, Figure S1) further suggest that the majority phase is anatase in accordance with the PEO predictions using the CSL assumption. We note, however, that such diffraction studies may be insufficient to rule out the presence of small rutile inclusions. Such rutile nanoparticle inclusions have been observed in similar work on (001)-oriented TiO_2 thin films;[20] however, the low volume fraction and varied orientation of such rutile nanocrystals preclude the ability to detect them by bulk diffraction methods, but they are present in transmission electron microscopy imaging. Nonetheless, these observations do not affect the current results as the majority phase is still anatase. This observation of epitaxially stabilized anatase to 900 °C even with a substrate−film lattice mismatch as high as 6.0% ($NdScO_3$) is somewhat surprising, but not completely unexpected. It has been observed previously that across various synthesis methods for both nanopowders and thin films, the anatase-to-rutile transition is highly variable, depending on, for example, nanocrystallite size, deposition rate, partial oxygen pressure, precursor solution, and substrate.[21−24] Our observation of the presence of predominantly anatase TiO_2 is further evidence of this variability and demonstrates the degree to which epitaxial stabilization is capable of skewing the energy landscape in thin films.

Additional information on the evolution of the energy landscape in this system requires that we consider other important energetic contributions. In particular, we focus here on the competition between bulk free and surface energies and how this evolves with the changing lattice mismatch including a brief discussion of the possible effect of strain on the initial nucleation and growth process. Prior work on epitaxial anatase has reported the observation of a characteristic morphology of densely arrayed epitaxially oriented nanocrystals of TiO_2 separated by antiphase boundaries (APB),[25−29] possibly due to the nucleation of the growing anatase unit cell at various locations along the *c* axis as a result of the 4_1 screw axis symmetry of anatase. Subsequent AFM scans of our films show the presence of such nanocrystals (Supporting Information, Figure S2). Recent in situ scanning tunneling microscopy studies of anatase films grown on Nb-doped $SrTiO_3$ substrates have unequivocally revealed the nature of nucleation and growth of anatase on perovskite substrates.[30] In particular, this work observed that an initially strained, wetting layer of anatase (two monolayers thick) is followed by island formation resulting in the characteristic nanocrystalline morphology. The current work also focuses on the growth of anatase on perovskite substrates, and thus we expect a similar growth process to occur with the added effect of increased strain energy for the initial wetting layers as the lattice mismatch is increased. From the AFM studies, we have extracted the average nanocrystallite diameter (*d*) of the TiO_2 using a line-trace method (ASTM Standard E112). From this analysis, it is seen that *d* scales inversely with lattice mismatch with the largest nanocrystals present on the most lattice-matched substrate ($LaAlO_3$) and the smallest on the most lattice-mismatched substrates ($GdScO_3$ and $NdScO_3$) (Figure 1d).

On the basis of this trend, we begin to understand the overall as-grown morphology, phase, and orientation within the context of the energy competition between strain energy density and the surface energy represented by the nanocrystallite diameter. Again, we observe that even at deposition temperatures 150 °C above the bulk anatase-to-rutile transition temperature, growth on (001)-oriented perovskite substrates preferably stabilizes anatase, despite lattice mismatches as large as 6.0%, due to the incredibly poor CSL for rutile. Additionally, the change in the preferred epitaxial orientation found to occur at ∼5% lattice mismatch is due to the competition in strain energy density between the 00*l*- and *h*00-orientations of anatase. Finally, the observed trend of decreasing nanocrystallite size with increasing lattice mismatch could potentially be explained by a number of factors. First, as the strain energy is increased (i.e., the lattice mismatch is increased), the nanocrystallite size decreases in an attempt to provide additional strain compensation to the system.[31−33] This added surface energy is accounted for by a reduction in strain energy, but throughout this evolution the epitaxial constraints keep the material in the anatase polymorph. One would expect a nearly linearly relationship in this case (see blue-dashed line, Figure 1d). A second possibility is that as the lattice mismatch increases there is change in the nature of growth in the material that results in a corresponding morphological change. For instance, as the strain gets larger, the critical thickness for the onset of Stranski−Krastanov growth may vary[34−37] or the growth may transform from a Stranski−Krastanov-like growth (as seen in the growth of anatase on $SrTiO_3$)[30] to a Volmer−Weber (or island) growth mode[34] as has been observed in other systems.[38−40] In either of these cases, a stepped dependence of the nanocrystallite size with lattice mismatch (where the number of wetted, strained layers jumps in integer multiples as strain moves across critical values) may be possible (see green-dashed line, Figure 1d). Unequivocal determination of which of these modes is responsible for the observed trends would require additional in situ characterization that is beyond the scope of the current work.

3.2. Structure and Orientation Changes from Annealing. Returning to the continuum elastic model, it is predicted that $GdScO_3$ is near the strain energy density crossover point making it difficult to predict the exact PEO, while *h*00 anatase is strongly favored for growth on $NdScO_3$. From the XRD experiments, we observed only 00*l*-oriented anatase on $GdScO_3$ and a mixture of 00*l*- and *h*00-oriented anatase on $NdScO_3$. We hypothesize that the nonequilibrium nature of the pulsed-laser deposition growth process may skew the energy landscape, thereby further promoting the stabilization of metastable structures in the films. Similar effects have been seen previously in the growth of epitaxial Cu_2O films and nanostructures on $SrTiO_3$ substrates wherein variation in the laser fluence, and therefore the adatom kinetic energy, can change the majority

dx.doi.org/10.1021/cg5000974 | Cryst. Growth Des. 2014, 14, 1981−1988

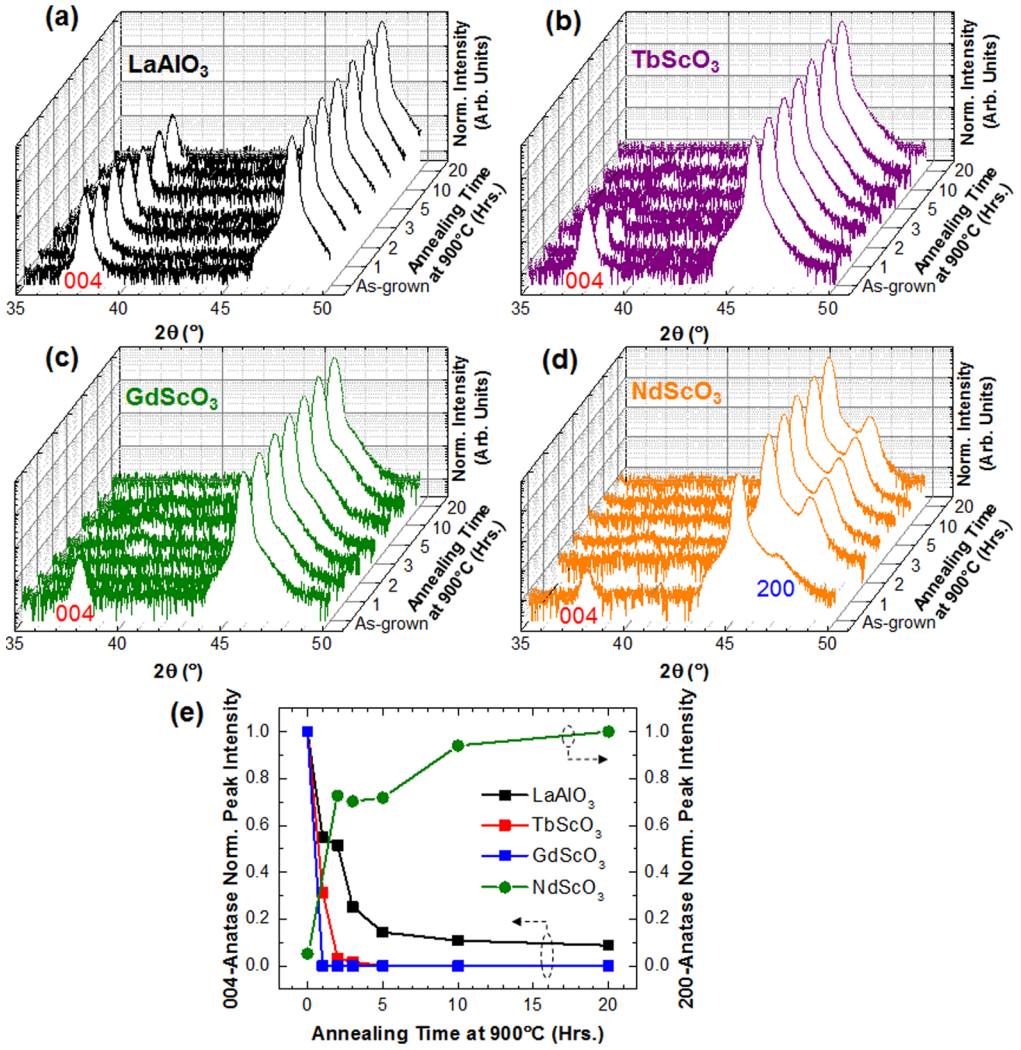

Figure 2. θ–2θ X-ray diffraction scans of following ex post facto annealing procedure for films grown on (a) $LaAlO_3$, (b) $TbScO_3$, (c) $GdScO_3$, and (d) $NdScO_3$ substrates. (e) Summary of the normalized peak intensity of the 004- and 200-diffraction conditions of anatase as a function of annealing time as extracted from (a–d).

facet and even the epitaxial orientation of the Cu_2O.[41] This added kinetic energy, in turn, can provide additional energy to overcome and adjust tendencies in the system. Such consideration would account for our observation of 00*l*-oriented anatase on $GdScO_3$ and $NdScO_3$ in which the small contribution of adatom kinetic energy is sufficient to stabilize the 00*l*-oriented anatase.

To test the stability of the as-grown orientation, phase, and morphology and to what extent the continuum elastic model is predictive, we conducted ex post facto annealing experiments at the growth temperature. Films on all substrates studied here were annealed at 900 °C in 760 Torr of oxygen for 1, 2, 3, 5, 10, and 20 h (sequentially). θ–2θ XRD scans (Supporting Information, Figure S3) were completed following each annealing step, and for brevity we provide that data for films on grown on $LaAlO_3$ (Figure 2a), $TbScO_3$ (Figure 2b), $GdScO_3$ (Figure 2c), and $NdScO_3$ (Figure 2d) substrates. A summary of the normalized anatase peak intensity as a function of annealing time is also provided (Figure 2e).

These results can be separated into three classes of behavior. First, in the case of TiO_2 films grown on $LaAlO_3$ and $TbScO_3$, we observe a gradual decrease in the intensity of the 004-diffraction condition of anatase with increasing annealing time. On the basis of the previous analysis of the energetic competition between strain energy density and surface area, we propose that the nanocrystallites of TiO_2 coarsen and that at a critical nanocrystallite size, corresponding to a critical surface energy, rutile nucleates on the anatase nanocrystal surface (as has been observed in transmission electron microscopy studies[42]). The lack of observable rutile peaks in the XRD scans results from the fact that the rutile is randomly oriented, and it occurs in relative small volumes for the annealing studies completed herein. We note that annealing at higher temperatures (up to 1200 °C) results in clear emergence of rutile diffraction peaks corresponding to randomly oriented versions of the material. Additionally, we observe that the loss of the diffraction peak intensity for 00*l*-oriented anatase is much more rapid for the films on $TbScO_3$ than on $LaAlO_3$, which we interpret as resulting from the influence of the larger mismatch, and thus higher strain energy density, which we propose lowers the critical surface energy for nucleation of rutile for TiO_2 films grown on $TbScO_3$ as compared to those grown on $LaAlO_3$.

Second, for films grown on $GdScO_3$, we observe a rapid and complete loss of the diffraction peak intensity for 00*l*-oriented anatase after even just 1 h of annealing at 900 °C. This can be understood by recalling that the continuum elastic model

dx.doi.org/10.1021/cg5000974 | *Cryst. Growth Des.* 2014, 14, 1981–1988

predicts that $GdScO_3$ falls at the strain energy density crossover point, which implies that there is no strong driving force to select one orientation over the other. In turn, the lattice mismatch has little role to play in quenching rutile formation, and thus rapid conversion is achieved.

Finally, for films on $NdScO_3$, we also observe a complete loss of the diffraction peak intensity for 00*l*-oriented anatase after just 1 h of annealing at 900 °C. Again, this is in agreement with the continuum elastic model prediction, which suggests that this orientation of anatase is no longer the lowest energy orientation. Unlike the films on other substrates, however, in the case of films on $NdScO_3$, the 200-diffraction peak of anatase is observed to increase in intensity throughout the annealing process, and no evidence of rutile formation is observed. We hypothesize that the annealing process provides ample energy to transform any metastable 00*l*-oriented anatase quickly to the lower energy *h*00-oriented anatase and that the close lattice matching of that orientation to the $NdScO_3$ stabilizes the film against transformation to rutile within the constraints of the annealing studies performed herein.

To summarize, the elastic constraints of the substrate, the nanocrystallite diameter, and the highly energetic nature of the growth process (i.e., the adatom kinetic energy) appear to come together to provide a complex evolution to the energy landscape of epitaxial TiO_2 grown on (001)-oriented perovskite substrates. In general, lattice mismatch or strain energy dominates unless it reaches large values where strain accommodation via nanocrystallite size and shape change can reduce that strain energy (partially) by creation of smaller features or modification of the nucleation and growth process. Additionally, when the strain energy difference between the two potential anatase orientations is small, additional energy sources (such as the adatom kinetic energy during the growth process) can provide a driving for the selection of one orientation over the other. Finally, the growth process produces metastable phases and morphological structures, and subsequent annealing can move the system toward overall global equilibrium in short order. In general, annealing tends to transform the anatase first to the PEO and then to nonepitaxial rutile given sufficient time (with the time to complete conversion scaling inversely with the lattice mismatch between the preferred anatase orientation and the substrate). The lattice and strain stabilization of anatase can be rather robust and can maintain anatase to temperatures well in excess of the bulk anatase-to-rutile transition temperature, and for some time at high temperatures before rutile eventually nucleates and subsequently grows at the expense of the anatase.

3.3. Morphology and Optical Property Changes.

Armed with this new insight into the relative competition between lattice mismatch or strain, bulk free, surface, and other energies in the system, we have gone on to explore how knowledge of the tendencies of this system can be used to deterministically manipulate the physical properties. TiO_2 is of course a widely studied material for solar-based applications (i.e., energy conversion and photocatalysis, environmental remediation, self-cleaning, etc.),[2,3] and paramount to these applications is the ability to enhance light absorption. With the insights gained from our studies, we now demonstrate a few pathways by which knowledge of the energy competition in epitaxial films of TiO_2 can be used to tune the morphology and optical properties. For brevity, we focus here on TiO_2 films grown on $LaAlO_3$ substrates as examples because of the close lattice match of the substrate to anatase (0.4% at substrate growth temperature, T_S), and the large optical band gap (~5.7 eV) of the substrate as compared to the film (3.2 eV).[43]

3.3.1. Effects of Growth Temperature (T_S). To understand the effects of temperature on the morphology and optical properties, we investigated the growth of TiO_2 films on $LaAlO_3$ at T_S = 600−900 °C, which spans a range of temperatures from 150 °C below to above the bulk anatase-to-rutile phase transition. While the gross structural properties (phase and epitaxial orientation as determined by XRD) of each of the films is the same as that reported above (i.e., fully 00*l*-oriented anatase films, akin to that reported in Figure 1b), the optical properties and morphology varied dramatically.

UV−visible transmission and reflection measurements were conducted and the absorption (%*A*) was found by %*A* = 100% − %*T* − %*R*, where %*T* is the transmission and %*R* is the total reflection (diffuse and specular) of the film where both %*T* and %*R* are normalized by measurement of the transmission and reflection of the $LaAlO_3$ substrate (Figure 3a). The results of

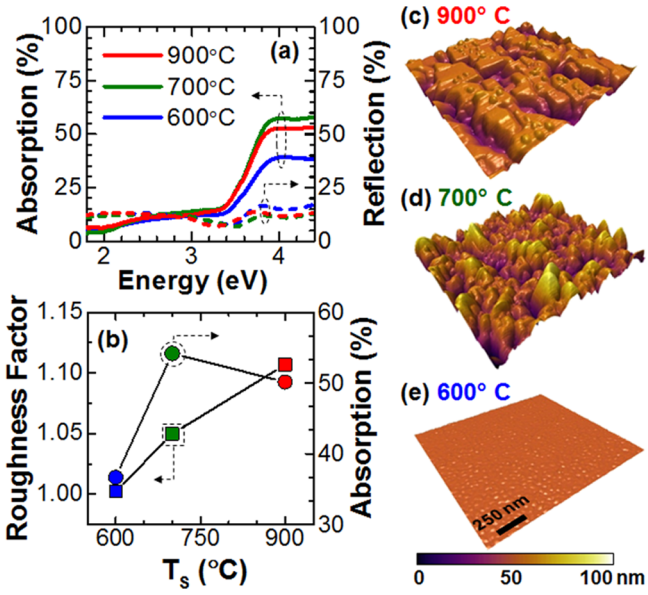

Figure 3. (a) Light absorption (solid lines) and reflection (dashed lines) and (b) roughness factor (f_r) (circles) and average above-band gap-energy light absorption (squares) as a function of growth temperature for anatase films grown on $LaAlO_3$ substrates. AFM morphology images of anatase films grown on $LaAlO_3$ substrates at T_S of (c) 900 °C, (d) 700 °C, and (e) 600 °C.

these studies revealed that above the band gap energy, the film grown at 600 °C possessed the highest reflection (15%) and lowest absorption (37%), while the films grown at 700 and 900 °C had the same reflection (10%) with the film grown at 700 °C having slightly higher absorption (54%) than the film grown at 900 °C (50%) (Figure 3b).

To help explain this trend and to investigate the influence of growth temperature on the microscale morphology, we measured the topography via AFM (Figure 3c−e). We observe that the morphology evolves from a faceted, nanocrystalline film exhibiting some amount of dewetting or island formation (henceforth referred to as island coarsening) from the substrate (T_S = 900 °C, Figure 3c) to a roughened, but wetted film (T_S = 700 °C) to a smooth film (T_S = 600 °C, Figure 3e). These observations may again be understood in terms of a competition among energies; however, in this case, because the films are grown on the same substrate, the difference in

dx.doi.org/10.1021/cg5000974 | Cryst. Growth Des. 2014, 14, 1981−1988

strain density between films grown at 600 and 900 °C is negligible (~2 mJ/cm^3). Also, on the basis of our previous observation of the epitaxial stabilization of anatase, we assume that the anatase-to-rutile phase transformation is quenched, and, therefore, we do not consider the bulk free energy. This leaves only three energies to be considered in the epitaxial TiO_2 thin film system: (1) the interfacial (chemical) energy between the substrate and the film, (2) the APB energy at the interface of nanocrystallites, and (3) the surface energy. While the lack of published values for either the interfacial or APB energy precludes a quantitative analysis, we present a qualitative discussion of the relative magnitudes of these three energies based on the morphological evolution of the films. We characterize the morphological evolution in terms of the change in normalized surface area as quantified by the roughness factor (f_r, defined as the measured surface area divided by the area of the AFM scan), the change in the nanocrystallite size, and the amount of island coarsening in the film.

For films grown at 600 °C, the films are continuous (wetted), f_r = 1.00, and $d \approx$ 58 nm, while for films grown at 700 °C, although the films remain continuous (wetted), f_r = 1.05, and $d \approx$ 61 nm. We surmise that the increase in the surface energy is less than the decrease in the APB energy and that there is no change in the interfacial energy. Upon moving to 900 °C, the increase in surface area and nanocrystallite diameter continues (f_r = 1.11, $d \approx$ 115 nm), and the films begin to dewet from the substrate. The island coarsening in the film has two effects: it decreases the film−substrate interface area and the APB area. We surmise from these changes that the increase in surface energy is less than the combined decrease in APB and interfacial energy.

These observed changes in the morphology also can be used to explain the observed changes in the light absorption. As T_S is increased from 600 to 700 °C, the increased roughness (1.3 and 11.6 nm root-mean-square (RMS), respectively) scatters more of the incident light, and thus the diffuse reflectance increases while the specular reflectance decreases, the net result of which is a small decrease in the total reflection and a larger increase in absorption resulting from the additional scattering at the surface. As the T_S is further increased from 700 to 900 °C, the emergence of the faceted nanocrystalline morphology increases the specular reflectance and decreases the diffuse reflectance, resulting in the total reflectance remaining unchanged and the absorption decreasing slightly as a combined effect of the decreased scattering of light at the surface and the island coarsening in the film.

In summary, the morphological evolution of the epitaxial anatase film grown on $LaAlO_3$ is explained by the energetic competition of the film−substrate interfacial energy, the nanocrystallite APB energy, and the surface energy. This competition results initially in a dramatic roughening of the film surface as T_S is increased from 600 to 700 °C, followed by the emergence of a faceted nanocrystalline morphology at 900 °C. The effect on the optical properties of the film is an increase in both the surface area and the light absorption. This would suggest that using a T_S = 900 °C would optimize the properties desired for light-based applications because at this growth temperature the film possesses high surface area, relatively high light absorption, and a large fraction of anatase (001) facets.

3.3.2. Effects of Annealing. With a reference point established for the change in morphology and optical properties with growth temperature, we proceed to investigate the effects of annealing the films. We chose the films grown at T_S = 900 °C based on our prediction that these films should possess the optimal properties for light-based applications. An annealing temperature of 900 °C was used in an attempt to minimize rutile formation during short annealing studies, thereby eliminating any convoluting factors during the evaluation of the light absorption.

Following the method described above, we measured the UV−visible transmission and reflection of the film in the as-grown state and after 1 and 2 h of total annealing time. The absorption and total reflection results are provided (Figure 4a)

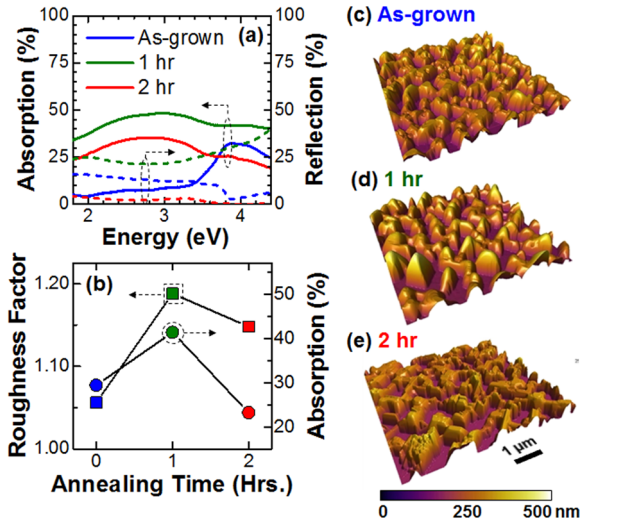

Figure 4. (a) Light absorption (solid lines) and reflection (dashed lines) and (b) roughness factor (f_r) (circles) and average above-band gap-energy light absorption (squares) as a function of annealing time at 900 °C for anatase films grown on $LaAlO_3$ substrates. AFM morphology images of anatase films grown on $LaAlO_3$ in the (c) as-grown state and after annealing for (d) 1 h and (e) 2 h.

and reveal that a 1 h annealing treatment results in a dramatic increase in the average above-band gap-energy reflection (5−33%) and a significant, but smaller, increase in the average above-band gap-energy absorption (34−40%). Upon annealing the film for a total of 2 h, the average above-band gap-energy reflection and absorption decrease to 1% and 25%, respectively (Figure 4b). We note that the apparent increase in the reflection and absorption below the band gap energy is an instrument artifact resulting from the significant increase in diffuse reflection and diffuse transmission which is not completely captured by the instrument.

To explain these observations, we again use AFM to study the evolution of the morphology (Figure 4c−e). In the as-grown state (Figure 4c), the film displays the characteristic faceted nanocrystalline morphology discussed above (note that the AFM scans in Figures 3c and 4c are on different scales to accommodate the morphology evolution with annealing time). After annealing the film for 1 h at 900 °C, the surface area has increased (f_r = 1.19), and additional island coarsening of the film is observed (Figure 4d). After 2 h of annealing at 900 °C, the film is observed to have undergone significant island coarsening, resulting in a decrease in the surface area (f_r = 1.15) (Figure 4e). From this trend, we can clearly see that the energetic competition of the film−substrate interfacial energy, the nanocrystallite APB energy, and the surface energy continues to drive the process of coarsening the nanocrystals.

dx.doi.org/10.1021/cg5000974 | *Cryst. Growth Des.* 2014, 14, 1981−1988

These observations also explain the trend in light absorption and reflection. Similar to the increase in growth temperature from 600 to 700 °C discussed in the previous section, the increase in roughness from the as-grown condition to after the 1 h anneal (8.1−97 nm RMS) results in increased scattering of the light at the surface and therefore increased reflection and absorption. Upon further annealing for a total of 2 h at 900 °C, the combination of decreased roughness (48 nm RMS) and increased film island coarsening results in the significant decrease in both the reflection and absorption.

Both higher growth temperature and longer annealing time produce the same change in morphology of epitaxial anatase and act to decrease the film-interface energy and APB energy at the expense of the surface energy. This difference in energies drives the roughening and coarsening of the nanocrystalline islands that comprise the film. The total change in morphology from growth at 900 °C plus 1 h of annealing at 900 °C has the net effect of increasing the surface area by ∼20% and increasing the light absorption above the band gap energy by ∼80% over an unannealed film grown at 600 °C. Such an increase in the surface area and light absorption is highly desirable for light-based applications of TiO_2.

4. CONCLUSION

In conclusion, we have used the concept of coincident site lattice matching to predict the preferred phase and orientation of TiO_2 on (001)-oriented perovskite substrates with lattice mismatches ranging from −2.0% to 6.0%. The epitaxial stabilization by the substrate permits anatase films to be grown at temperatures at least 150 °C above the bulk anatase-to-rutile phase transition temperature. Using a continuum elastic model, we calculated the strain energy density for 00*l*- and *h*00-oriented anatase as a function of lattice mismatch and find that it predicts a crossover in preferred orientation at a lattice mismatch of ∼5.0%. Subsequent experimental studies confirm these predictions and added energies are found to be involved in the evolution of film phase, orientation, and morphology. For instance, TiO_2 nanocrystallite size is found to decrease with lattice mismatch and is attributed to partial compensation of the strain energy with surface energy and/or to a change in the nucleation and growth process. When the strain energy difference between the two orientations of anatase is small, energy contributions from other sources (in the form of adatom kinetic energy from the growth process) can also impact epitaxial orientation. To further probe the competition between bulk free, surface, interface, and strain energies in metastable (kinetically limited) as-grown TiO_2 films, in situ growth processes and ex post facto annealing studies were completed to assess the equilibrium state of the films. These studies confirm the continuum elastic model and highlight the relative importance of the different energies. In particular, we observe that the evolution of the film morphology with increasing growth temperature and annealing time reveals that a decrease in film−substrate interface energy and antiphase boundary energy occurs at the expense of an increase in surface energy driving the nanocrystalline anatase islands to coarsen and possibly dewet from the substrate. Leveraging this understanding of the competing energetics, we demonstrate the ability to increase the surface area by 20% and the light absorption (above the band gap energy) by 80%. This work provides further insight into the nature of epitaxial growth of TiO_2 and serves as a template for improving the properties of this important material in light-based applications.

■ ASSOCIATED CONTENT

Ⓢ Supporting Information

Figure S1. Pole figure scans (showing only one quadrant of the 4-fold symmetric scans) for a $TiO_2/LaAlO_3$ (001) heterostructure. Figure S2. Atomic force microscopy (AFM) images of the as-grown TiO_2 thin films. Figure S3. $\theta-2\theta$ X-ray diffraction studies of the ex post facto annealing studies of TiO_2 films. This material is available free of charge via the Internet at http://pubs.acs.org.

■ AUTHOR INFORMATION

Corresponding Author

*E-mail: lwmartin@illinois.edu.

Notes

The authors declare no competing financial interest.

■ ACKNOWLEDGMENTS

The authors gratefully acknowledge support by the International Institute for Carbon-Neutral Energy Research (WPI-I2CNER), sponsored by the Japanese Ministry of Education, Culture, Sport, Science and Technology. Experiments were carried out in part in the Materials Research Laboratory Central Facilities.

■ REFERENCES

(1) DeVries, R. C.; Roy, R. *Am. Ceram. Soc. Bull.* **1954**, *33*, 370−372.
(2) Fujishima, A.; Zhang, X.; Tryk, D. A. *Surf. Sci. Rep.* **2008**, *63*, 515−582.
(3) Carp, O.; Huisman, C. L.; Reller, A. *Prog. Solid State Chem.* **2004**, *32*, 33−177.
(4) *National Bureau of Standards (U.S.) Monograph*; National Bureau of Standards: Gaithersburg, MD, 1969; Vol. *25*, pp 82−83.
(5) Silva, V. F.; Bouquet, V.; Députier, S.; Boursicot, S.; Ollivier, S.; Weber, I. T.; Silva, V. L.; Santos, I. M. G.; Guilloux-Virya, M.; Perrina, A. *J. Appl. Crystallogr.* **2010**, *43*, 1502−1512.
(6) Makino, M.; Matsumoto, Y.; Nakajima, K.; Makino, T.; Segawa, Y.; Chikyow, T.; Ahmet, P.; Kawasaki, M.; Koinuma, H. *Appl. Phys. Lett.* **2001**, *78*, 2664−2666.
(7) Gorbenko, O. Yu.; Samoilenkov, S. V.; Graboy, I. E.; Kaul, A. R. *Chem. Mater.* **2002**, *14*, 4026−4043.
(8) Ong, C. K.; Wang, S. J. *Appl. Surf. Sci.* **2001**, *185*, 47−51.
(9) Lotnyk, A.; Senz, S.; Hesse, D. *Thin Solid Films* **2007**, *515*, 3439−3447.
(10) Tao, J.; Luttrell, T.; Batzill, M. *Nat. Chem.* **2011**, *3*, 296−300.
(11) Lina, H.; Rumaiz, A. K.; Schulz, M.; Wang, D.; Rock, R.; Huang, C. P.; Shah, S. I. *Mat. Sci. Eng. B-Solid* **2008**, *151*, 133−139.
(12) Schultz, A. M.; Zhu, Y.; Bojarski, S. A.; Rohrer, G. S.; Salvador, P. A. *Thin Solid Films* **2013**, *548*, 220−224.
(13) Matěj, Z.; Kužel, R.; Nichtová, L. *Metall. Mater. Trans. A* **2011**, *42A*, 3323−3332.
(14) Aggarwal, R. L.; Ripin, D. J.; Ochoa, J. R.; Fan, T. Y. *J. Appl. Phys.* **2005**, *98*, 103514.
(15) Chakoumakos, B. C.; Schlom, D. G.; Urbanik, M.; Luine, J. *J. Appl. Phys.* **1998**, *83*, 1979−1982.
(16) Chaix-Pluchery, O.; Chenevier, B.; Robles, J. J. *Appl. Phys. Lett.* **2005**, *86*, 251911.
(17) de Ligny, D.; Richet, P. *Phys. Rev. B* **1996**, *53*, 3013−3022.
(18) Uecker, R.; Velickov, B.; Klimm, D.; Bertram, R.; Bernhagen, M.; Rabe, M.; Albrecht, M.; Fornari, R.; Schlom, D. G. *J. Cryst. Growth* **2008**, *310*, 2649−2658.
(19) Rao, K. V. K.; Naidu, S. V. N.; Iyengar, L. *J. Am. Ceram. Soc.* **2006**, *53*, 124−126.
(20) Chambers, S. A.; Wang, C. M.; Thevuthasan, S.; Droubay, T.; McCready, D. E.; Lea, A. S.; Shutthanandan, V.; Windish, C. F., Jr. *Thin Solid Films* **2002**, *418*, 197−210.

(21) Ranade, M. R.; Navrotsky, A.; Zhang, H. Z.; Banfield, J. F.; Elder, S. H.; Zaban, A.; Borse, P. H.; Kulkarni, S. K.; Doran, G. S.; Whitfield, H. J. *Proc. Natl. Acad. Sci., U. S. A.* **2002**, *99* (suppl. 2), 6476−6481.
(22) Zhang, H.; Banfield, J. F. *J. Mater. Chem.* **1998**, *8*, 2073−2076.
(23) Tang, H.; Prasad, K.; Sanjinbs, R.; Schmid, P. E.; Lévy, F. *J. Appl. Phys.* **1994**, *75*, 2042−2047.
(24) Yu, J.-G.; Yu, H.-G.; Cheng, B.; Zhao, X.-J.; Yu, J. C.; Ho, W.-K. *J. Phys. Chem. B* **2003**, *107*, 13871−13879.
(25) Ashbee, K. H. G.; Smallman, R. E.; Williamson, G. K. *Proc. R. Soc. London A* **1963**, *276*, 542−552.
(26) Bursill, L. A.; Hyde, B. G. *Proc. R. Soc. London A* **1970**, *320*, 147−160.
(27) Reece, M.; Morrell, R. *J. Mater. Sci.* **1991**, *26*, 5566−5574.
(28) Liang, Y.; Gan, S.; Chambers, S. A.; Altman, E. I. *Phys. Rev. B* **2001**, *63*, 235402.
(29) Tanner, R. E.; Sasahara, A.; Liang, Y.; Altman, E. I.; Onishi, H. *J. Phys. Chem. B* **2002**, *106*, 8211−8222.
(30) Du, Y.; Kim, D. J.; Kaspar, T. C.; Chamberlin, S. E.; Lyubinetsky, I.; Chambers, S. A. *Surf. Sci.* **2012**, *606*, 1443−1449.
(31) Kern, R.; Müller, P. *J. Cryst. Growth* **1995**, *146*, 193−197.
(32) Henry, C. R. *Prog. Surf. Sci.* **2005**, *80*, 92−116.
(33) Müller, P.; Kern, R. *Surf. Sci.* **2000**, *457*, 229−253.
(34) Eaglesham, D. J.; Cerullo, M. *Phys. Rev. Lett.* **1990**, *64*, 1943−1946.
(35) Venables, J. A. *Surf. Sci.* **1994**, *299/300*, 798−817.
(36) Tersoff, J.; LeGoues, F. K. *Phys. Rev. Lett.* **1994**, *72*, 3570−3573.
(37) Tabuchi, M.; Noda, S.; Sasaki, A. *J. Cryst. Growth* **1991**, *115*, 169−173.
(38) Leonard, D.; Krishnamurthy, M.; Reaves, C. M.; Denbaars, S. P.; Petroff, P. M. *Appl. Phys. Lett.* **1993**, *63*, 3203−3205.
(39) Tu, Y.; Tersoff, J. *Phys. Rev. Lett.* **2004**, *93*, 216101.
(40) Cullis, A. G; Norris, D. J.; Walther, T.; Migliorato, M. A.; Hopkinson, M. *Phys. Rev. B* **2002**, *66*, 081305(R).
(41) Lee, S.; Liang, C. W.; Martin, L. W. *ACS Nano* **2011**, *5*, 3736−3743.
(42) Gouma, P. I.; Mills, M. J. *J. Am. Ceram. Soc.* **2001**, *84*, 619−622.
(43) Peacock, P. W.; Robertson, J. *J. Appl. Phys.* **2002**, *92*, 4712−4721.